공학박사학위논문

표면 플라즈몬에 의해 증폭된 Fin Ge-Si 발광 다이오드의 설계와 분석

Design and Analysis of Surface Plasmon-enhanced Fin Ge-Si Light-emitting Diode

2014년 8월

서울대학교 대학원
융합과학부 나노융합전공
정 인 태

Abstract

Design and Analysis of Surface Plasmon-enhanced Fin Ge-Si Light-emitting Diode

Intae Jeong

Program in Nano Science and Technology

The Graduate School

Seoul National University

Si photonics is a filed of studying integrating photonic devices into CMOS chip. All photonic components including modulators, waveguides, detectors are already available commercially but efficient group IV compatible on-chip light sources are still studied in academic world. Fortunately, heavily-doped strained Ge can emit light efficiently thanks

to its pseudo direct band gap characteristic. This makes Ge a good candidate for on-chip monolithic light sources in Si photonics systems. In this paper, we propose fin-shaped Ge-Si heterojunction LED with metal gates, which can enhance light emission by coupling with surface plasmon resonant modes and modulate light emission from the LED. This enhancement effect is called the Purcell effect. Due to this effect, the spontaneous emission rate of an emitter can be changed by its environment like metal cavity. In our device, this effect is caused by surface plasmon in metal surface. We calculate this enhancement effect in our fin device, and show that a certain dimension of device can maximize the spontaneous emission. We thoroughly investigate the physical aspect of various 1D multilayer system to understand the physics of the surface plasmon effect in depth. We also check the possibility of gate modulation in both two aspect, i.e electrical modulation and optical modulation. By device simulation we can see the electrical modulation is possible and the modulation speed can reach 5 GHz. We conduct experiment using surface plasmon resonance sensor to check the possibility of the optical modulation. We applied voltage on the metal electrode and measure the SPR angle difference. We construct a model to explain our result and apply this model to the fin

LED. This reveals that the gate bias hardly affect on enhancement factor, that is the optical modulation is not possible. This study will help in design and optimization of light sources including surface plasmon enhanced LED and nanocavity laser for on-chip light sources in Si photonics.

Keywords : Surface plasmon resonance, Purcell effect, Gate modulation, Si photonics, Germanium light source

Student Number : 2009-30731

Contents

List of Figures

Chapter 1. Introduction

1.1 Why Si photonics?

Until now, optical communication thorough optical interconnect has only limited application, usually for long distance range communication. Optical communication has advantages such as broad bandwidth and low loss but complicated and expensive electric-optical conversion system is needed. For short range distance communication, electrical interconnect has been used because it is cheap and can be integrable in a small area. However, as integrated circuits (ICs) are scaled down following Moore's law, challenges in data communication through electric interconnects are arising due to bandwidth limit [1-4]. Even in short distance level communications such as chip-to-chip and intra-chip communication, optical interconnects become increasingly necessary to overcome this bottleneck. This is why Silicon (Si) photonics, which is the discipline of integrating optical components on a complementary metal-oxide-semiconductor (CMOS) chip, is considered as a solution of the bandwidth problem in future ICs.

In state-of-the-art Si photonics technology, nearly all optical components such as modulators [5, 6], detectors [7], waveguides and nonlinear elements [8] have been well implemented monolithically except an efficient light source (Fig. 1.1). Currently, III-V semiconductor based external light sources are used mainly in Si photonics systems. Another solution is to construct a hybrid device like III-V semiconductor based vertical-cavity surface-emitting lasers on a silicon-on-insulator substrate [9, 10]. This is because group IV materials like Si and Germanium (Ge) have indirect band gaps while other semiconducting materials like GaAs have direct band gaps, showing superior light emitting property compared to indirect band gap semiconductors. However, if we can make use of group IV semiconductors as light-emitting materials, the manufacturing process can be cheaper and easier because it is more compatible with the well-established Si-based process than hybrid devices manufacturing processes.

Si photonics system are already commercially available by various company such as Intel, Luxtera, etc (Fig. 1.2(a)). Also, Samsung electronics is trying to make Si photonics system using bulk Si process, not SOI, for future DRAM interface. IBM is also planing to make one

chip that is integrated CPU, and RAM, photonics system in layered structure (Fig. 1.2(b)).

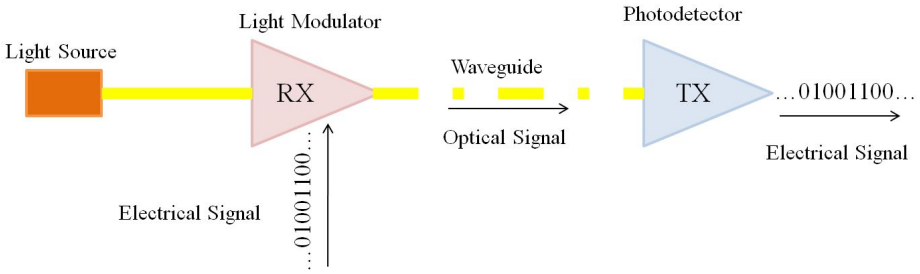

Fig. 1.1 Usual Si photonics system. A light source (external LED or laser) emit continuous light. A light modulator (usually Si modulator) receives digital electronic and change continuous light to digital optical signal. This optical signal follows through Si waveguide and Ge photodetector receives it and transforms it into the original electrical signal.

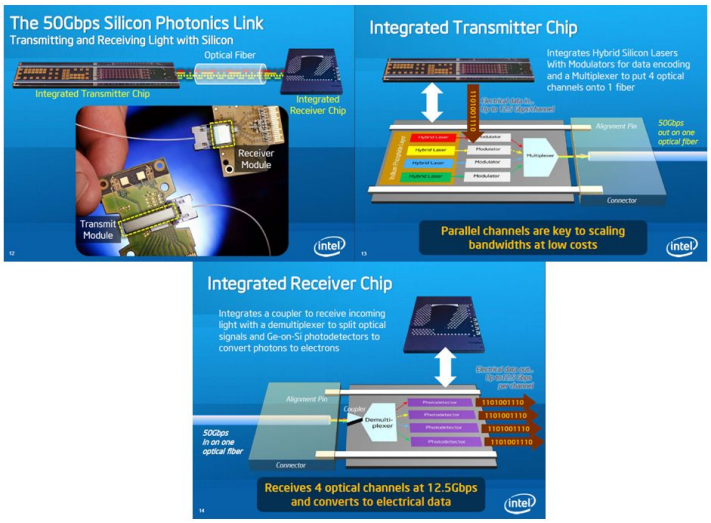

(a)

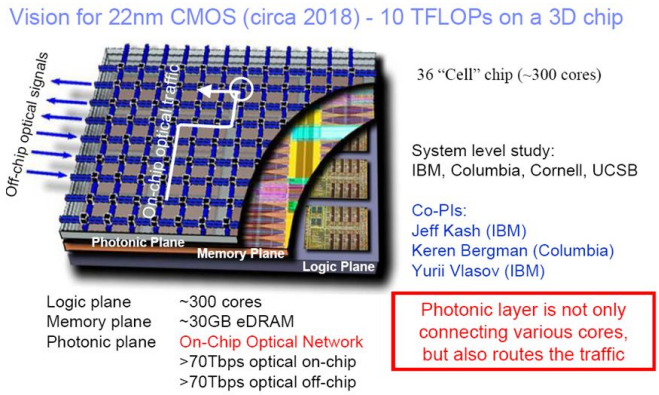

(b)

Fig. 1.2 Efforts to make Si photonics system by main IT companies. (a) Intel has implemented usable high speed Si photonics system. They achieve 50 GHz photonic link through one optical fiber by means of 4-channel WDM (wavelenghth division modulation). (b) IBM vision for future high performance computer using Si photonics. CPU plane, RAM plane, and optical interconnect planes are stacked and integrated one chip.

1.2 Ge as on-chip light source

Recently, it has been proved that Ge can be used as an efficient light emitting material for on-chip monolithic light sources [11, 12]. Ge lasers [13] and light-emitting diodes (LEDs) [14, 15] (Fig. 1.3(a) and (b)) were already demonstrated and actively studied. To make Ge a good light emitting material, band structure engineering of Ge is needed by means of controlling the lattice constant. Ge has a pseudo direct band gap behavior because the energy difference between the indirect conduction valley (the L-valley) and the direct conduction valley (the Γ -valley) is relatively small (only 0.136 eV, Fig. 1.4(a)). For this reason, Ge has been used in some photonic devices like Ge photodetectors. J. Liu et al. showed tensile-strained and heavily doped n-type Ge is more likely to have direct-band-gap-like property thanks to the Γ-valley lowering [11]. Strained Ge can be obtained by epitaxial growth on a Si substrate. Due to the lattice mismatch, tensile stress is applied to the Ge epilayer on the Si substrate and gives tensile strain to make the lattice constant of Ge large, resulting into lowering of the energy level of the Γ-valley. Also, heavy n+ doping on Ge can increase electron population on the Γ-valley, which can further enhance the direct recombination. Strain larger than 2% can eventually make Ge a true

direct band gap material, but dramatic energy band gap narrowing occurs (Fig. 1.4(b)) [16]. Weak and moderate straining on Ge does not alter the energy band gap significantly (0.664 eV, light emission of 1550 nm wavelength) and it still takes advantage of the Γ-valley lowering to become more direct-band-gap-like. About 0.2% strain on Ge is widely used for this reason [13-15]. By counting the electron population in each valley with the Fermi-Dirac statistics, the possible maximum internal quantum efficiency (q, Fig. 1.4(c)) of 0.2% strained and heavily n+ doped (~1019/cm3) Ge is calculated to be approximately 10% [17]. But this is an ideal value. The actual value of q is smaller than the calculated value and depends on a defect condition in the Ge epilayer [12].

If we could increase q by enlarging radiative recombination rate γr which corresponds to the spontaneous emission rate, Ge can emit light with improved efficiency. In this paper, we propose a fin type device structure with metal gates and show that we can obtain an enhanced γr and the q, thereby more light emission, by surface plasmon mode coupling in the cavity of the metal gates. We conduct a rigorous numerical analysis to obtain a device structure for maximizing the light emission. For various values of quantum efficiency without the enhancement effect, and for various types of gate metal, the optimal device structure and specific device dimensions can be obtained. In

addition, device simulations show that light modulation is possible by simply modulating the gate voltage on the metal gate. The modulating speed of the device can reaches 5 GHz.

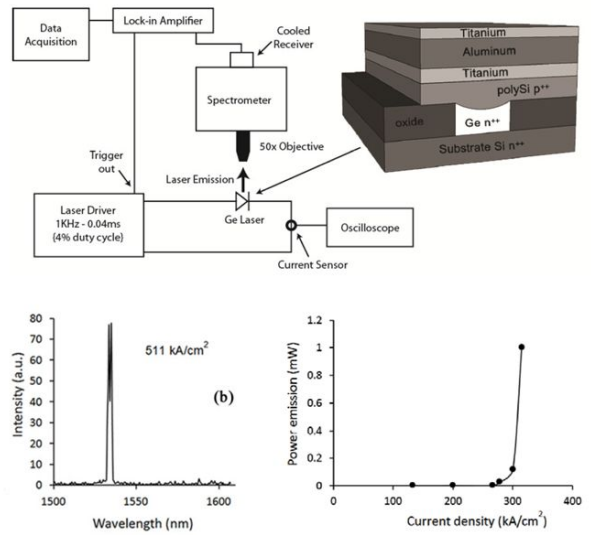

(a)

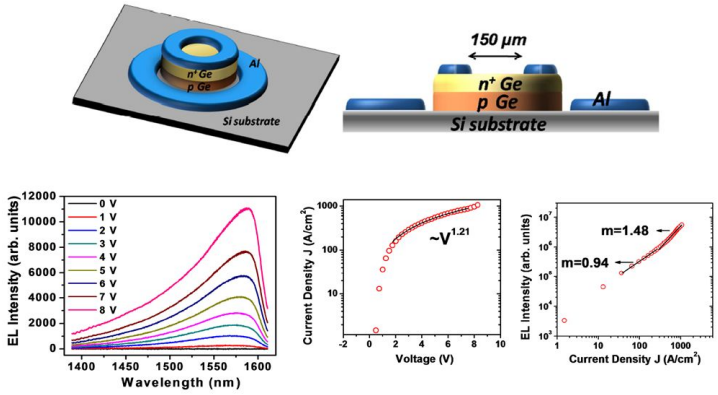

(b)

Fig. 1.3 Implemented Ge light sources (a) Ge laser [13] (b) Pillar Ge LED [14]

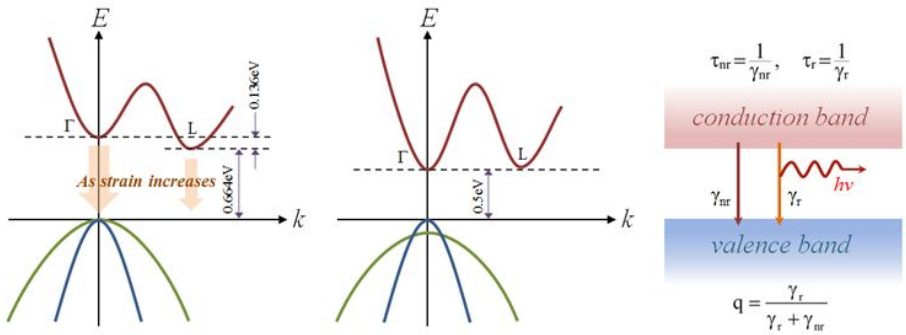

(a) (b) (c)

Fig. 1.4 Energy band structure of Ge under straining [11]. (a) Energy band structure of unstrained bulk Ge. The band gap is 0.664 eV. It is an indirect band gap. The energy difference between the Γ-valley and the L-valley is relatively small (0.136 eV). By addressing tensile strain, Ge can be more direct-band-gap-like due to lowering of the Γ-valley. The L-valley also becomes lower, yet slower than the Γ-valley lowering. (b) 2% strain makes Ge a true direct band gap material by lowering the Γ-valley down to the L-valley level. Valence band structure also changes slightly. The band gap energy becomes much smaller. (0.5 eV) (c) Recombination processes. γ_r is the radiative recombination rate and γ_{nr} is the nonradiative recombination rate. Each lifetime (τ_{nr} and τ_r) is the reciprocal of each rate. Internal quantum efficiency q is the ratio of γ_r to the total recombination rate, $\gamma_r + \gamma_{nr}$.

1.3 Proposal of surface plasmon-enhanced fin Ge-LED

Here we propose a new LED design (Fig. 1.5(a)) which has fin Ge-Si heterojunction p-n diode structure [18]. This device inherently has a small footprint by adopting a fin structure. The fin Ge-Si LED is sandwiched by two metal film gates to form a plasmonic nano cavity consisting of a metal-dielectric-metal waveguide structure. The heavily doped n+Ge region is the light emitting part. As forward bias V_d is applied, holes injected from the p-Si region recombine with electrons in the n+Ge region by both the radiative and nonradiative processes (Fig. 1.5(b)). The metallic film is the most crucial part for the working of the device. It can enhance light emission of the LED by coupling with the surface plasmonic resonant modes [19-21]. This is due to an optical cavity effect called the Purcell effect, which explains the phenomena that the spontaneous emission can be changed by surrounding environment [22]. Nanophotonic environments such as photonic crystal constructing photonic band structures [23] and metal interface causing surface plasmon resonance [19-21] can alter the spontaneous emission rate of a light emitter in those environments. Also, the metal gates can be used to modulate the injection of the carriers in the LED. Thus it can be used as a switch and a modulator. When the gate bias V_g on

both metal gates is applied, the potential barrier for holes in the Ge region will obstruct hole transport through the p-n diode (Fig. 1.5(c)). Furthermore, this device can be used as a photodetector. It means that this device can be used for both the transmitter (LED) and the receiver (photodetector) in one form.

For the respective dimensions of the device, the height of the fin (600 nm) is properly chosen to reduce defects in Ge. The most area of the fin is composed of Ge (500 nm) because it is the light emitting region. The oxide thickness t_{ox} is also determined for proper passivation from the metal gates and for moderate plasmon effect. If t_{ox} is too thin, light emission near the metal gates is absorbed by the metal and does not radiate out to the free space due to dissipation by Joule heating. This phenomenon is called the quenching which is a loss [24]. The quenching effect is not significant if we set t_{ox}=5 nm, which also gives good gate controllability. Other dimensions of the structures such as the thickness of Ge t_{Ge} and the thickness of the metal gate t_m are variables.

This device can be built on a standard CMOS wafer with well-established manufacturing processes as follows (Fig. 1.6) : first, Ge is grown epitaxially on a p-doped Si substrate. Ge is in-situ doped by n-type impurities during the growth process. After the fin array is patterned by etching process, deposition of oxide follows. Metal gate is

deposited on both side of the fin. Transparent contact like indium tin oxide (ITO) for Ge electrode may be deposited above the device after filling the empty space between the fin arrays.

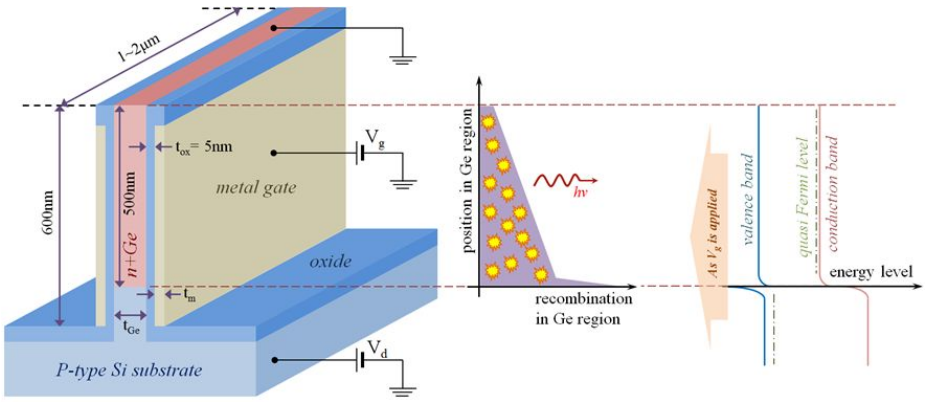

(a) (b) (c)

Fig. 1.5 Fin Ge-Si LED (a) Structure of fin Ge-Si LED. Metal gates on both sides can enhance radiative recombination rate in the Ge region and modulate light. Diode forward bias is Vd and gate bias on both metal gates is Vg. (b) Recombination rate in the Ge region. Some of electron-hole pairs are eliminated by recombination and emit photons. Light emission rate is proportional to q. (c) Energy band diagram when Vd is applied. If we apply Vg, the whole energy band becomes lower, presenting an energy barrier for holes.

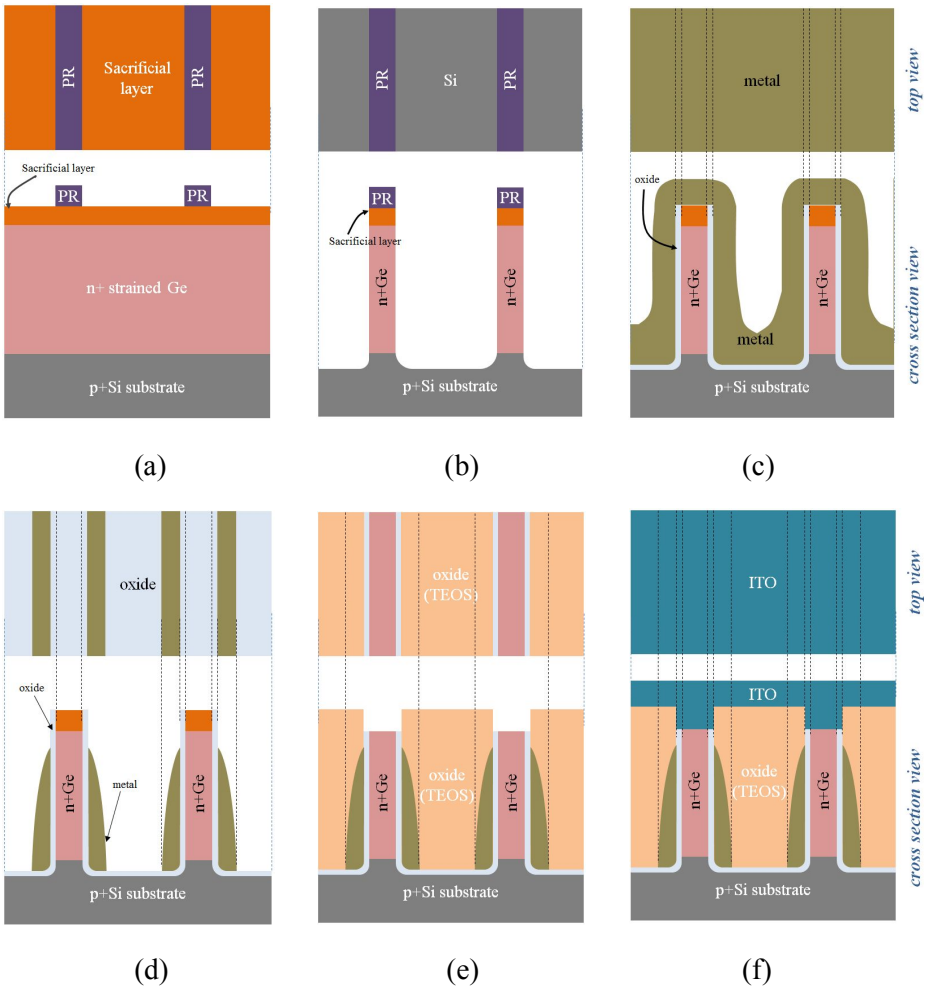

Fig. 1.6 Brief device manufacturing process sequence (a) n+Ge deposition on p+Si substrate making mask (b) Etching out to make fin structure (c) Metal deposition (d) Metal etch back to form metal plasmonic gate (e) Gap filling (oxide) and removing the sacrificial layer (f) Transparent electrode (ITO) deposition

Chapter 2. Theory and Formalism

2.1 The Purcell effect

Edward Mills Purcell (1912~1997, Fig. 2.1(a)) is famous as a Nobel prize for physic laureate for his NMR study in 1952. He also discovered so-called the Purcell effect in 1946. At that time, spontaneous emission rate was considered as a inherent property of a emitter. From elementary quantum mechanics theory, we know that energy eigenstates are stationary state and if an external excitation is absent, the system's state keeps maintained. Actually spontaneous emission is not explained by the elementary quantum mechanics until 1946. Purcell discovered that the spontaneous emission rate of an emitter is not a constant value and it depends on its environment. An emitter in cavity, its spontaneous emission rate γ enhances by the Purcell factor E in cavity environment (Fig. 2.1(b)). Purcell suggested that E is given in this equation.

$$E = \frac{3}{4\pi^2}\left(\frac{\lambda_c}{n}\right)\frac{Q}{V} \tag{1}$$

Q is cavity Q-factor and V is the modal volume. λ_c is the wavelength

and n is mode number.

After quantum electrodynamics (QED) developed in 1950's, the physics of spontaneous emission was revealed finally, and the Purcell effect E can obtained rigourously. Spontaneous emission is caused by external excitation even in vacuum by vacuum field fluctuation. If an emitter is in specific environment, the interaction between the emitter and its surrounding environment can enhance or suppress the spontaneous emission rate. This effect can be calculated from QED theory. First, by Fermi's golden rule the spontaneous emission rate γ is proportional to the local photonics density of states (LPDOS) ρ at $\boldsymbol{r_0}$ like this equation.

$$\gamma = \frac{2\omega\pi}{3\hbar\varepsilon_0}|p|^2\rho \tag{2}$$

ω is the optical frequency, ħ is the Planck constant, ε_0 is the vacuum permittivity, and p is the dipole strength. LPDOS can be obtained from system's dyadic Green's function $\vec{\vec{G}}(\boldsymbol{r},\boldsymbol{r}')$ from this equation.

$$\rho = \frac{\omega}{\pi c^2} Tr\left(\mathrm{Im}\left\{\vec{\vec{G}}(\boldsymbol{r_0},\boldsymbol{r_0})\right\}\right) \tag{3}$$

$\vec{\vec{G}}(\boldsymbol{r},\boldsymbol{r}')$ is the solution set at $\boldsymbol{r}$ of Maxwell's equation, for point oscillating dipole source at $\boldsymbol{r}'$ i.e this equation.

$$\nabla\times\nabla\times\vec{\vec{G}}(\boldsymbol{r},\boldsymbol{r}') - \frac{\varepsilon\omega^2}{c^2}\vec{\vec{G}}(\boldsymbol{r},\boldsymbol{r}') = \vec{\vec{I}}\delta(\boldsymbol{r}-\boldsymbol{r}') \tag{4}$$

By finding the ratio LPDOS in eq. (2) of an emitter in a certain environment to an emitter in vacuum environment, we can obtain the Purcell factor E in more rigorous way than Purcell's way.

From above method, we can calculate the emission enhancement in any photonics environment, such as photonic crystal (PC) and metal interface. Especially an emitter near metallic surface can enhance its radiation by coupling with surface plasmon resonance mode.

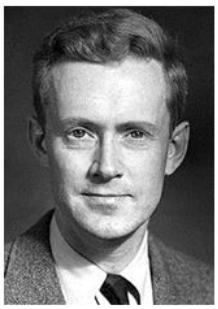

Edward Mills Purcell (1912~1997)

(a)

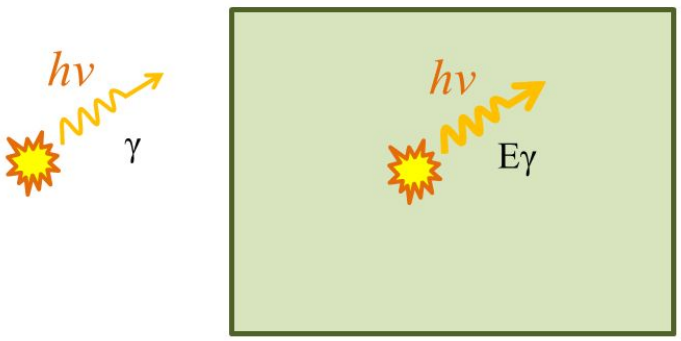

(b)

Fig. 2.1 Purcell effect (a) Edward Mills Purcell (b) A simple illustration of the Purcell effect. An emitter in vacuum radiate right by spontaneous emission. The spontaneous emission rate is γ. (left) Another emitter in cavity can emit more light. The spontaneous emission rate is enhanced by the Purcell factor E.

2.2 Surface plasmon

Surface plasmon (SP) is an special mode of electro-magnetic (E/M) wave which propagate through the interfacial surface between metal and dielectric. In metal surface at the interface, plasma wave of free electron (plasmon) couples with the E/M wave in dielectric region. If the wave vector of external excitation matches with that of SP mode, surface plasmon resonance (SPR) can occurs, and external excitation can give rise SP mode.

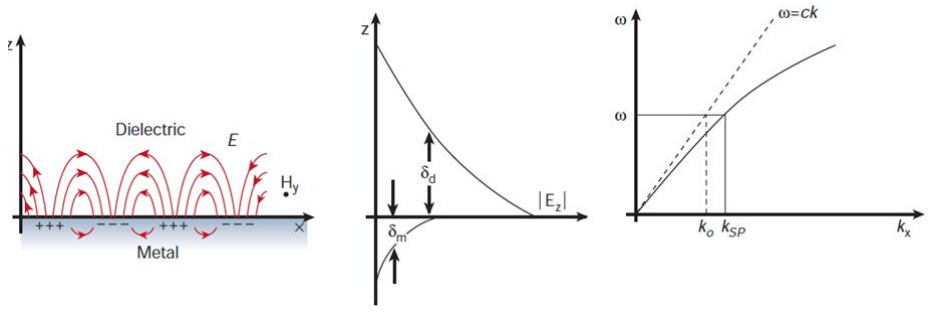

(a) (b) (c)

Fig. 2.2 Surface plasmon (a) Electric field profile of a certain SP mode. It is a TM wave (b) Energy distribution of the SP mode. In metal it decays exponentially. Its characteristic length is the skin depth. (c) Dispersion reation of the SP mode. It has larger wave vector compared to the free space wave. It is due to lagging effect of free electron wave.

2.3 Spontaneous emission calculation

To determine t_{Ge} and $t_{m,}$ we performed a numerical analysis for the emission property of an emitter in the Ge region to maximize the surface plasmon coupling and enhance the spontaneous emission rate. For the calculation of the E, we assume our structure as a one-dimensional (1D) multilayer system (Fig. 2.3). This can be justified because the aspect ratio of our device is relatively large and the wavelength of surface plasmonic mode is short compared to the fin height [26].

The delta function source in eq. (4) represents an oscillating dipole in the multilayer system. To obtain the dyadic Green's function in the 1D multilayer system analytically, each term in eq. (4) is transformed by the spatial Fourier transform, from functions of position $\mathbf{r}$ = (x, y, z) to functions of wave vector $\mathbf{k}$ = (k_x, k_y, k_z). It means that the dyadic Green's function can be represented as the superposition of plane waves propagating in all directions. k is decomposed into the in-plane component $\mathbf{k}_{\parallel}$ = (k_x, k_y, 0) and the normal component $k_{\perp}$ = (0, 0, k_z). The integral through the normal component k_z can be removed if we obtain the reflectivities of both the upper and the lower layers of the

multilayer system ($R_{\uparrow}$ and $R_{\downarrow}$ in Fig. 2.3(b)). Hence the final form of the dyadic Green's function, and hence the LPDOS, are represented as integrals over the magnitude of in-plane wave vector $|\mathbf{k}_{\parallel}|$ = $k_{\parallel}$. From the calculated dyadic Green's function of the 1D multilayer system, the LPDOS can be written as [30, 31]

$$\rho = \frac{\omega}{4\pi^2 c^2}\int_0^{\infty} dk_{\parallel}\,\mathrm{Re}\left\{\left(\frac{k_{\parallel}}{k_{\perp}}\eta_1^{S}\right)+\left(\frac{k_{\parallel}k_{\perp}}{k^2}\eta_2^{P}\right)+\left(\frac{k_{\parallel}^3}{k^2 k_{\perp}}\eta_1^{P}\right)\right\} \tag{5}$$

Each η is a function of $R_{\uparrow}$ and $R_{\downarrow}$ for each s and p polarization at the emission site (Fig. 2.3(b)). They are represented as

$$\eta_1^{P} = \frac{(1+R_{\uparrow})(1+R_{\downarrow})}{1-R_{\uparrow}R_{\downarrow}},\quad \eta_2^{P} = \frac{(1-R_{\uparrow})(1-R_{\downarrow})}{1-R_{\uparrow}R_{\downarrow}},\quad \eta_1^{S} = \frac{(1+R_{\uparrow})(1+R_{\downarrow})}{1-R_{\uparrow}R_{\downarrow}} \tag{6}$$

The reflectivities for each polarization can be calculated from the transfer matrix method (explained in next section) [30, 31]. These reflectivities account for the emission enhancement through constructive interference by the phase coincidence between the emitter and reflected lights.

Since γ_r is proportional to the LPDOS (by Fermi's golden rule, eq. (2)), E near the metal gate can be calculated by obtaining the ratio of the LPDOS for a certain device dimensions (t_m and t_{Ge}) to the LPDOS without enhancement in the bulk Ge. Eq. (5) means the LPDOS for certain wavelength can be considered as a density spectrum of the

in-plane wave vector. In this spectrum, the region where the magnitude of the in-plane wave vector k|| is smaller than the magnitude of the wave vector |k| = k can be interpreted as directional emission (going to $\theta = \sin^{-1}(k||/k)$) of free space waves. If $k_{||}$ is larger than k, then this gives imaginary $k_{\perp}$ which corresponds to plane-bounded surface plasmonic modes.

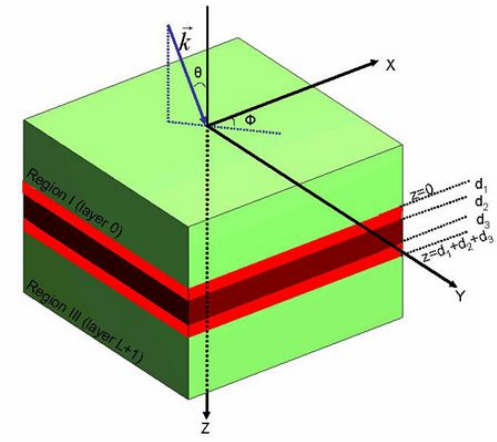

(a)

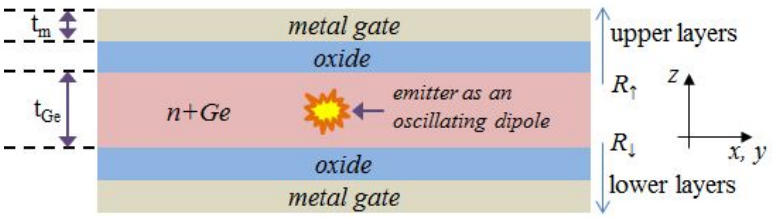

(b)

Fig. 2.3 1D multilayer system (a) General 1D multilayer system (b) 1D multilayer system which represents our fin Ge-Si LED

2.4 Transfer matrix method

For 1D multilayer system (Fig 2.4), the reflectivity which is needed in eq. (6) can be obtained from the transfer matrix method.

For each interface between any two layer, transitivity and reflectivity for each s and p polarization can be obtained using this equation.

$$t_{s,n-1\leftarrow n} = \frac{2k_{z,n}(\lambda, k_{xy})}{k_{z,n}(\lambda, k_{xy}) + k_{z,n-1}(\lambda, k_{xy})} \tag{7}$$

$$r_{s,n-1\leftarrow n} = \frac{k_{z,n}(\lambda, k_{xy}) - k_{z,n-1}(\lambda, k_{xy})}{k_{z,n}(\lambda, k_{xy}) + k_{z,n-1}(\lambda, k_{xy})} \tag{8}$$

$$t_{p,n-1\leftarrow n} = \frac{2k_{z,n}(\lambda, k_{xy})\epsilon_{n-1}(\lambda)}{k_{z,n}(\lambda, k_{xy})\epsilon_{n-1}(\lambda) + k_{z,n-1}(\lambda, k_{xy})\epsilon_n(\lambda)} \tag{9}$$

$$r_{p,n-1\leftarrow n} = \frac{k_{z,n}(\lambda, k_{xy})\epsilon_{n-1}(\lambda) - k_{z,n-1}(\lambda, k_{xy})\epsilon_n(\lambda)}{k_{z,n}(\lambda, k_{xy})\epsilon_{n-1}(\lambda) + k_{z,n-1}(\lambda, k_{xy})\epsilon_n(\lambda)} \tag{10}$$

From eq. (7)~(10), interfacial transfer matrix **I** for any interface can be represented as

$$\mathbf{I}_{s(p);n-1,n}(\lambda, k_{xy}) = \begin{bmatrix} \frac{1}{t_{s(p),n-1\leftarrow n}(\lambda,k_{xy})} & \frac{r_{s(p),n-1\leftarrow n}(\lambda,k_{xy})}{t_{s(p);n-1\leftarrow n}(\lambda,k_{xy})} \\ \frac{r_{s(p);n-1\leftarrow n}(\lambda,k_{xy})}{t_{s(p),n-1\leftarrow n}(\lambda,k_{xy})} & \frac{1}{t_{s(p),n-1\leftarrow n}(\lambda,k_{xy})} \end{bmatrix}. \tag{11}$$

And the propagation transfer matrix through any layer **P** is represented

as

$$\mathbf{P}_n(\lambda, k_{xy}) = \begin{bmatrix} \exp(-jk_{z,n}d_n) & 0 \\ 0 & \exp(jk_{z,n}d_n) \end{bmatrix}. \quad (12)$$

The system's whole transfer matrix can be obtained by multipling all the interface and propagation transfer matrix sequencially like this.

$$\begin{bmatrix} A_{s(p),\downarrow,n} \\ A_{s(p),\uparrow,n} \end{bmatrix} = \mathbf{L}_{s(p);,N+1}(\lambda, k_{xy}) \ldots \mathbf{L}_{s(p),n}(\lambda, k_{xy}) \ldots \mathbf{L}_{s(p),1}(\lambda, k_{xy}) \begin{bmatrix} A_{s(p),\downarrow,0} \\ A_{s(p),\uparrow,0} \end{bmatrix} \quad (13)$$

each L in this equation is

$$\mathbf{L}_{s(p),n}(\lambda, k_{xy}) = \mathbf{P}_n(\lambda, k_{xy}) \cdot \mathbf{I}_{s(p),n-1,n}(\lambda, k_{xy}) \quad (14)$$

We can obtain the system's whole reflectivity and transitivity from this equation.

$$\begin{bmatrix} r_{s(p),0\leftarrow N+1}(\lambda, k_{xy}) \\ 1 \end{bmatrix} = \mathbf{L}_{s(p),N+1} \ldots \mathbf{L}_{s(p),n} \ldots \mathbf{L}_{s(p),1} \begin{bmatrix} 0 \\ t_{s(p),0\leftarrow N+1}(\lambda, k_{xy}) \end{bmatrix} \quad (15)$$

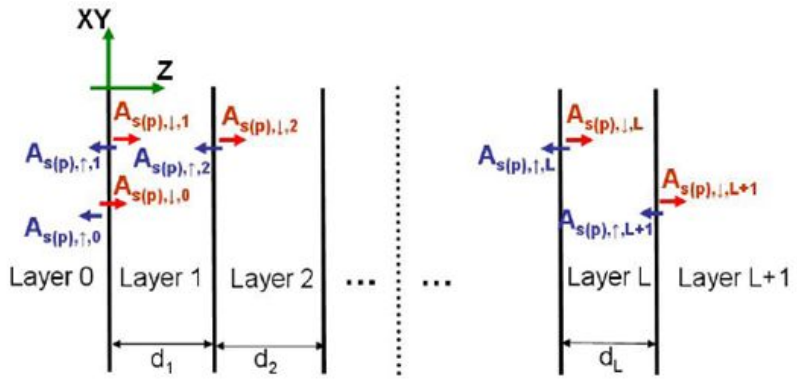

Fig. 2.4 1D multilayer system to illustrate the transfer matrix method

Chapter 3. Analysis Results and Discussion

3.1 Optimization of device design

The Purcell effect only affects γ_r by a factor of the Purcell enhancement factor E, and decreases τ_r, not altering the γ_{nr} (Fig. 1.3(c)). γ_r becomes $E\gamma_r$, enhancing the internal quantum efficiency accordingly [25]. If the quantum efficiency without the Purcell effect is $q_0 = \gamma_r / (\gamma_r + \gamma_{nr})$ (hereafter called the intrinsic internal quantum efficiency), then the enhanced q can be expressed as a function of E and q_0 as

$$q(E, q_0) = \frac{E\gamma_r}{E\gamma_r + \gamma_{nr}} = \frac{Eq_0}{1 + q_0(E-1)} \quad . \tag{16}$$

The q vs. E with q_0 as a parameter is depicted in Fig. 3.1(a). As examples with the points marked with 'x' in the figure, if q_0 of strained Ge is 1 %, (this means the ratio of γ_r to γ_{nr} is 1:99) and γ_r is enhanced by a factor of 100 (E = 100), γ_r : γ_{nr} becomes 100:99 and q becomes about 50 %. If q_0 is 10 % and E is 100, then the q becomes about 91 %.

We consider the light with the wavelength of 1550 nm, which is

the emission peak of strained Ge [11]. First, we calculate E with varying t_m and t_{Ge} for an emitter located at the center of the multilayer. With the calculated E, we can obtain the enhanced quantum efficiency from $q = q(E, q_0)$ in eq. (16) for a certain value of q_0. We suppose the total emission is given by $q(E, q_0)t_{Ge}$. This holds if the current density is same for various t_{Ge}, and if $q(E, q_0)$ for the whole fin area is same. It includes the propagation loss of surface plasmonic guided modes. The total emission for a device with the gold (Au) gate is depicted in Fig. 3.2(a) for several q_0, i.e. 1%, 5%, and 10% which is the theoretical maximum. As q_0 increases, the maximum emission point occurs at thicker t_{Ge}. This is because t_{Ge} becomes more dominant than q for devices with higher q_0. From this data we can choose the optimal device dimension maximizing the total emission (x-points in Fig. 3.2(a)). The graph in Fig. 3.1(b) justifies the assumption that E is invariant under the emitter position; as the dipole location deviates from the center of the fin, E does not vary significantly. Fig. 3.2(c) shows the total emission with various gate metals (silver (Ag), aluminum (Al), and tungsten (W)) when q_0 is 5 %. It shows similar patterns with Fig. 3.2(a). To design the optimal device, we should properly choose the device dimension (t_m , t_{Ge}) for a given q_0 and material for the metal gate.

We can see interesting points when we carefully investigate and compare the LPDOS density spectrum of the in-plane wave vector (the integrand in eq. (5)) for metal-less and metal-gated structures. Before the metal gate is deposited, there is no LPDOS portion in the surface plasmon region where the in-plane wave vector magnitude is larger than the magnitude of the wave vector. As t_m is increased from 0 to 1.5 nm, the surface plasmonic portion in the LPDOS density spectrum dramatically emerges while free-space wave component is not changed significantly (the top graph of Fig. 3.3(a)). E versus t_m is depicted in Fig. 3.3(b) with the points denoting the data in Fig. 3.3(a). The total area bounded by curves in the top graph of Fig. 3.3(a) corresponds to the points marked with 'o' in Fig. 3.3(b) (normalized to the LPDOS for bulk Ge). t_{Ge} is fixed to 30 nm. E is maximized at t_m = 1.5 nm. As t_m increases further, the area bounded by LPDOS density shrinks, resulting into decreased LPDOS and E. The peaks of the LPDOS spectrum in the surface plasmon region are coincident with the surface plasmonic guided modes (the bottom graph of Fig. 3.3(a)) which are calculated by finding the minimum of the reflectivity of the whole multilayer system [33]. Two peaks correspond to even (Fig. 3.4(a)) and odd (Fig. 3.4(b)) plasmonic modes, respectively. It indicates that the energy from the emitter near metal is efficiently transferred to those

modes by near-field coupling. Also it means that enhancement of γ_r by constructing another radiative reaction path which is caused by the surface plasmon polariton coupling. Electric field profile of the even surface plasmonic mode (Fig. 6(a), bottom) is depicted in Fig. 3.3(c). The wavelength of this plasmonic mode is 170 nm and typically short compared with free space wavelength (1550 nm) as already mentioned. Several wavelengths can come inside to seemingly short fin height (600 nm). This fact justifies the 1D multilayer approximation.

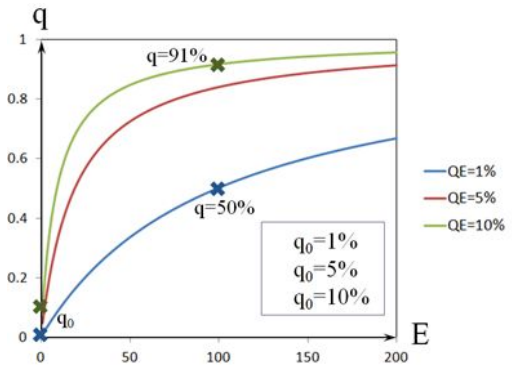

(a)

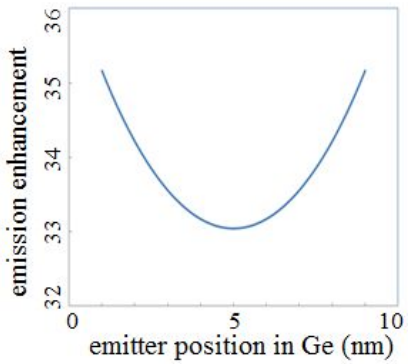

(b)

Fig. 3.1 (a) Quantum efficiency q enhanced by the enhancement γ_r of for various intrinsic q_0. E is the enhancement factor, i.e. the Purcell factor. (b) Emitter position in the Ge layer vs. E for t_m=2 nm and t_{Ge}=10 nm with Au gate. It is almost invariant as the emitter position is varied. It is similar for other device dimensions (not shown).

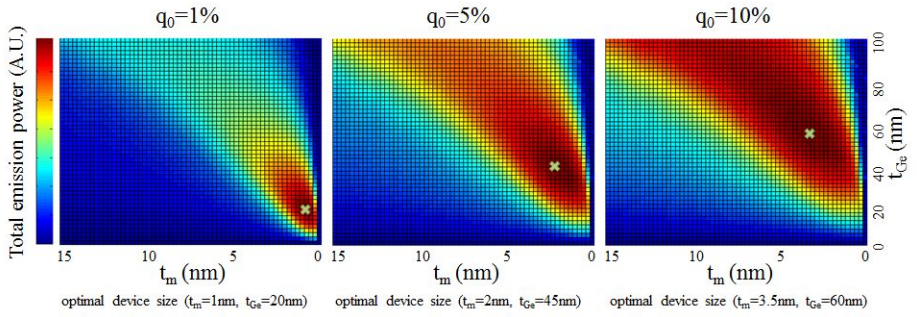

(a)

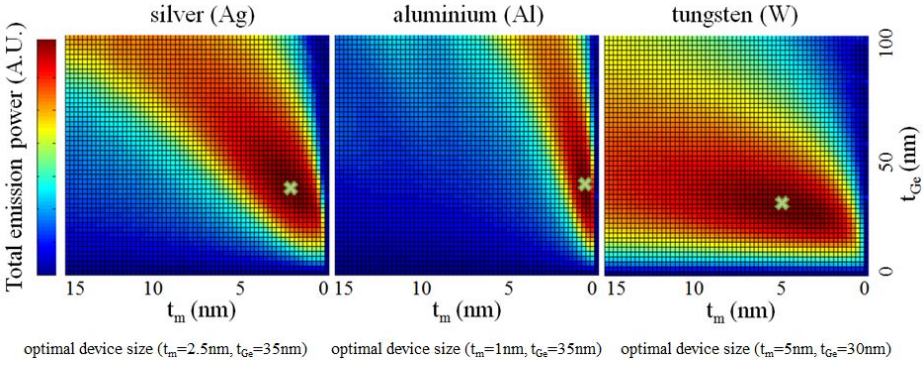

(b)

Fig. 3.2 (a) The total emission power vs. (t_m , t_{Ge}) for several q_0 with Au gate. The optimal device dimensions maximizing the total emission are indicated for each q_0 (x-points). (b) Total emission power for different metal gates. (q_0 = 5 %)

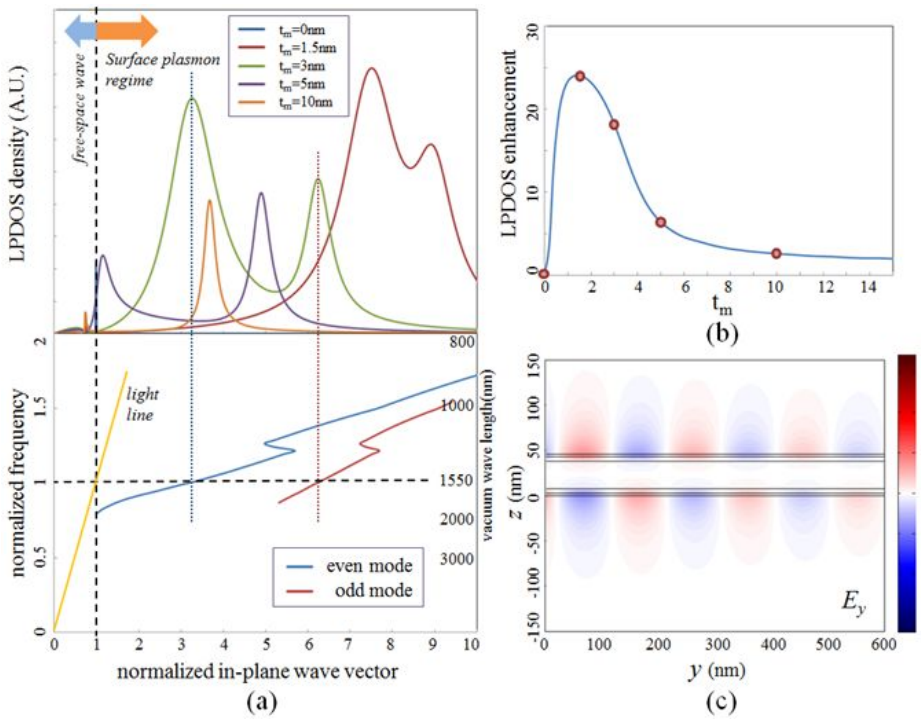

Fig. 3.3 (a) Top : LPDOS density spectrum per in-plane wave vector. Metal gate gives rise to surface plasmonic mode (t_m = 0, 1.5, 3, 5, 10 nm , t_{Ge} = 30 nm). Bottom : dispersion relation when t_m = 3 nm. Peaks in the LPDOS density coincides with the propagation modes. $k_{||}$ is normalized to the magnitude of k in the oxide. (b) E vs. t_m with t_{Ge} = 30 nm. Various t_m points in (a) are indicated as o-points (c) E-field profile (E_y) of the even surface plasmonic mode when t_m = 3 nm and t_{Ge} = 30 nm.

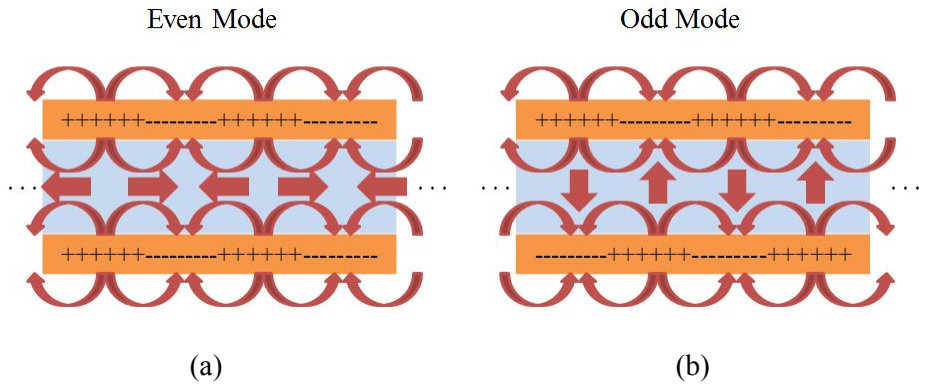

Fig. 3.4 Even and odd mode filed profile scheme (a) Even plasmonic mode in metal-dielecttric-metal system (b) Odd plasmonic mode filed profile.

3.2 Investigation of gate modulation – electrical

In our fin Ge LED, volatage bias in metal gate can modulate light source (Fig. 3.5(a)). Electric modulation is possible as mentioned in introduction. Optical modulation caused by altering of permittivity of the metal by E-filed excition may be possible. We will check both possibility. In this section we will focus on the electical modulation.

For the electrical simulation to see the controllability of metal gate potential to the carrier injection, the Sentaurus device simulation tool with standard device simulation models has been used [32].

Device simulation results to see the gate modulation of the carrier injection, thereby the light modulation are in Fig. 3.6. When V_d is applied on the GeSi p-n diode (Fig. 1.5(a)), positive V_g raises the potential barrier of holes in the diode (Fig. 1.5(c)), inhibiting the p-n diode current accordingly. This gate modulation effect is much more dominant in the p-i-n diode (100 nm of intrinsic Ge is inserted between p-Si and n+Ge in the fin LED) than p-n diode (Fig. 3.6(a)). This is because the energy barrier is modulated more easily in the undoped region. All previous optical optimization analysis is still applicable for the p-i-n structure because doping on Ge does not change the optical property significantly. We cannot completely turn off the diode because gate bias just raises the energy barrier without

blocking all the carrier transfer. Gate modulation works well for thinner t_{ox} (Fig. 3.6(b)) and t_{Ge} (Fig. 3.6(c)) due to easier electric field penetration. Fig. 3.6(d) shows the transient response of current when an on-off pulse signal is applied. For diode on-off mode, the off-state is V_d=0 V and the on-state V_d=0.7 V. V_g is fixed to 0 V. For gate on-off mode, the off-sate is V_g=1 V and the on-state is V_g=0 V. V_d is fixed to 0.7 V this time. Both modulations by the gate voltage and the diode voltage are possible and show similar responses. Considering the rising time and the falling time of the transient response, the maximum modulation speed is calculated to be about 5 GHz.

When we check the energy band diagram for on, off state in p-n (Fig. 3.7(a)) and p-i-n (Fig. 3.7(b)) LED, we can see why p-i-n diode is more easily gate-controllable. For p-n LED, hole energy barrier is not successfully constructed, but in p-i-n LED hole barrier is dramatically formed in intrinsic region. To investigate the cross section of the energy barrier for p-i-n diode in intrinsic region (Fig. 3.7(c)), we can see the energy barrier is higher as the distance from the metal is closer (Fig. 3.7(d)).

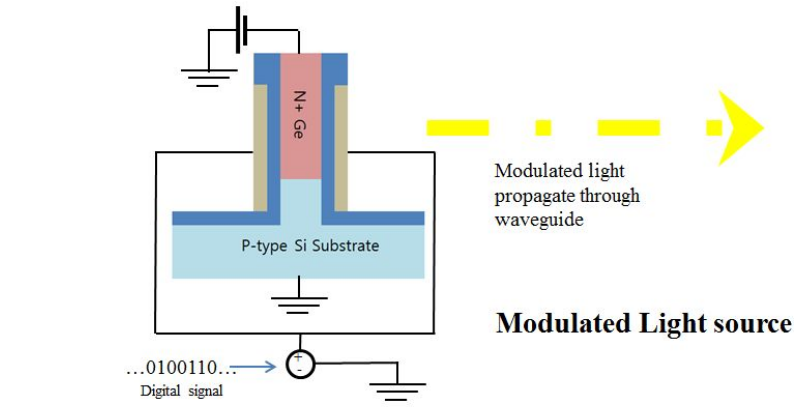

(a)

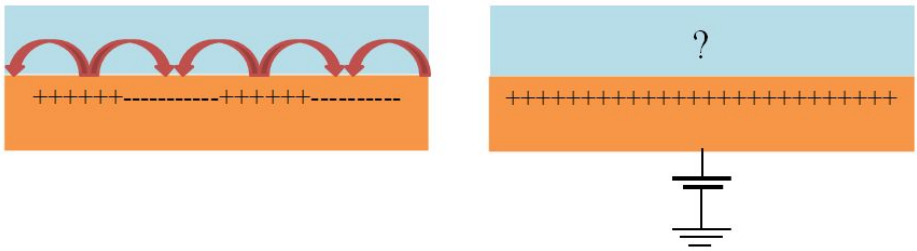

Floating or no bias

DC bias

(b)

(c)

Fig. 3.5 Moduation of fin LED (a) Gated modulation scheme. Digital signal from gate voltage can generate modulated light. (b) Field profile of plasmonic mode. At the metal surface, density wave of electron couple with E/M wave in dielectric region (c) when metal surface is biased, surface charge will be accumulated on the metal surface and SPR mode can possibly be changed.

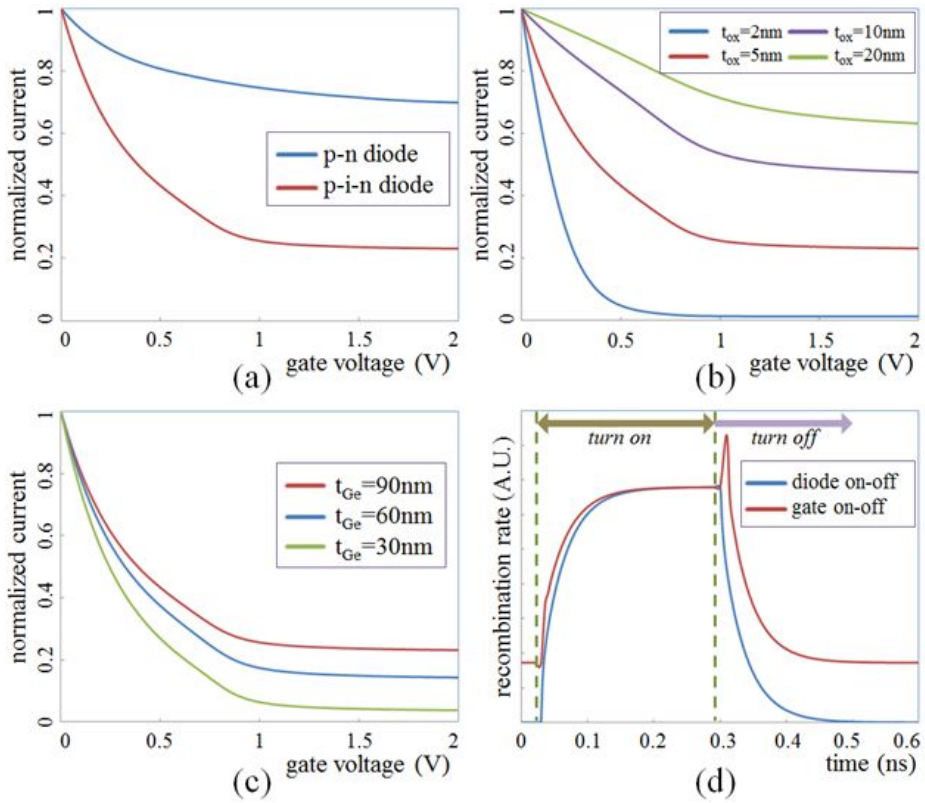

Fig. 3.6 Electrical simulation results. The oxide thickness is all 5nm as in Fig. 2(a) except in case of (c). (a) Current normalized to gate-off current vs. positive gate bias. p-i-n diode has better gate controllability then p-n diode. (b) As tox decreases, the gate controllability improves. (tGe=90 nm) (c) Thinner tGe has better gate modulation capability. (d) Transient responses of pulse input. ((b)~(d) are results for for p-i-n diode.)

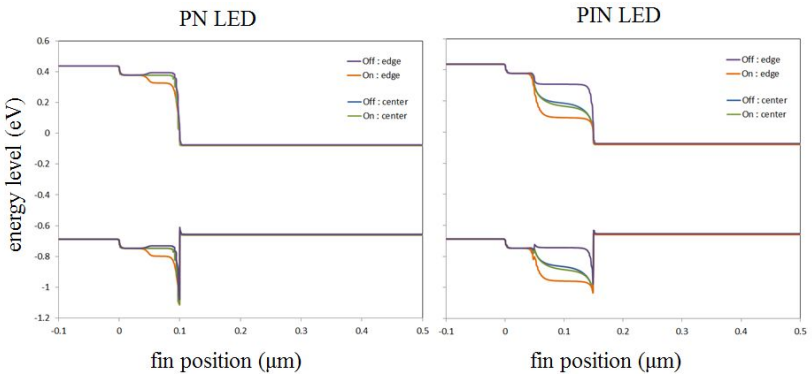

(a) (b)

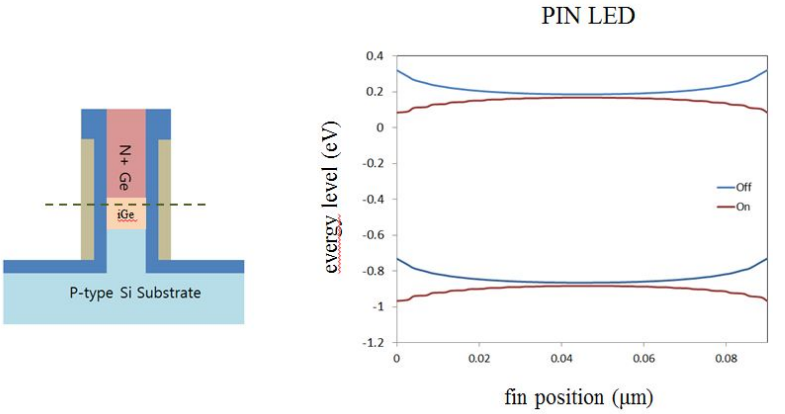

(c) (d)

Fig. 3.7 Energy band for modulation (a) Energy band diagram for p-n diode in each on-off mode and, at the center and edge region. The energy barrier for hole is not high to turn off the diode (b) Energy band diagram for p-i-n diode in each on-off mode and, at the center and edge region. The energy barrier for hole is high enough to turn off the diode. (c) Cross section of in intrinsic region of p-i-n fin LED. (d) Energy band for each gate on-off mode. The energy barrier is higher in the edge region. Only holes near edge can be blocked while holes in the center can pass through.

3.3 Investigation of gate modulation – optical

We conduct experiment using an SPR (surface plasmon resonance) sensor to verify optical modulation aspect. Fig 3.8(a) is SPR sensor from MiCoBioMed co.,ltd. The wavelength of the light source is a 685nm laser. Fig 3.8(b) is a schematic diagram of a SPR sensor. Light ray of various incident angles from an external light source is incident to the metal surface. For the light component whose in-plane wave vector component coincides with SP mode, SPR occurs and this light component is absorbed. The angle of this light component (θ) is the SPR angle of the system. If biomolecules are attached to the metal surface, the change of permittivity above the metal surface alters the SPR angle. If we measure this SPR angle change, biomolecules can be sensed. This is the working principle of SPR sensors.

Fig 3.9(a) shows schematic diagram of the experimental sample. Electrolyte layer is enveloped between two metal films (gold) which forms a capacitor structure. If we apply voltage (Va) between the metal layers, the SPR angle changes slightly from θ to θ'. The equivalent circuit is depicted. When we apply step-function-like voltage, the transient responses of current are like these (Fig 3.9(b)). By integrating

the transient response of current except constant current component, surface charge (Q_s) and surface charge density (σ_s) can be obtained Fig 3.9(c).

Experiment results are shown in Fig 3.10. Fig 3.10(a) depict voltage on the metal film vs. SPR angle shift for various pH buffer solution. The slope of each curve differs apparently. For the relation between surface charge density angle SPR angle shift, they become almost coincident compared to the above graph (Fig 3.10(b)). For low value of σ_s (<120μC/cm^2), they appear to be linear. For higher value of σ_s (>120μC/cm^2), the slope decreases.

Previous model which explains this effect is the SCL (space charge layer) model [39-41]. This is the assumption that surface charge on the metal is distributed thin SCL (about 1Å) The surface charge density $\sigma_s$alter the electronic density in SCL by Δn like this equation.

$$\Delta n = \frac{\sigma_s}{de_0} \tag{17}$$

d is the thickness of SCL (1Å in the previous model), e_0 is the charge of an electron. The change of electron density changes the permittivity of SCL given by

$$\Delta\varepsilon = (1-\varepsilon_f)\frac{\Delta n}{n} \tag{18}$$

where n is the density of free electron (for gold, it's 5.9x10^{20}m^{-3}), ε_f is

free electron contribution of the permittivity of metal given by the Drude model. This is like this equation.

$$\varepsilon_f = 1 - \frac{\omega_p^2}{\omega^2 - i\omega/\tau} \tag{19}$$

ω is the angular frequency of the light, and τ is the relaxation time of free electrons in gold (9.3×10^{-15}sec). ω_p is plasma frequency which is obtained from

$$\omega_p = \sqrt{\frac{ne_0^2}{\varepsilon_0 m}} \tag{20}$$

Here, ε_0 is the vacuum permittivity, m is the mass of an electron. If apply the change of permittivity in SCL, we can obtain the SPR angle shift. This can be found by calculation of the minimum of the reflectivity of the multilayer system from the transfer matrix method in section 2.4.

Fig 3.11(a) is the experiment results and SPR angle shift obtained from theoretical model. Previous SCL model can only explain a part of linear region (σs <50μC/cm2). A low peak emerges near σ_s =70μ C/cm^2. Furthermore, in the non-linear region, the curve of previous SCL model diverges faster than curves from experimental data. The modified SCL model is well agreed with experiment result. (b) The pseudocapacitor model. Excessive surface charges (σ_s>120μC/cm^2) are

accumulated in the oxide layer as protons, not in SCL.

From the modified SCL model, we find that previous SCL model is still applicable in our fin LED. If we apply this model to our LED (Fig 3.12), optical modulation effect is shown to be not significant. To modulate by gate voltage biasing, we only need to consider electric modulation aspect.

(a)

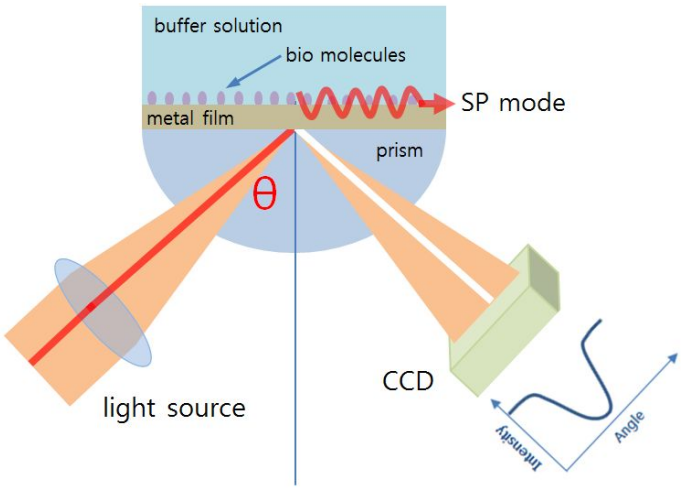

(b)

Fig. 3.8 SPR sensor scheme (a) An SPR sensor from MiCoBioMed which we used for our experiment to verify optical modulation. (b) Working principle of an SPR sensor.

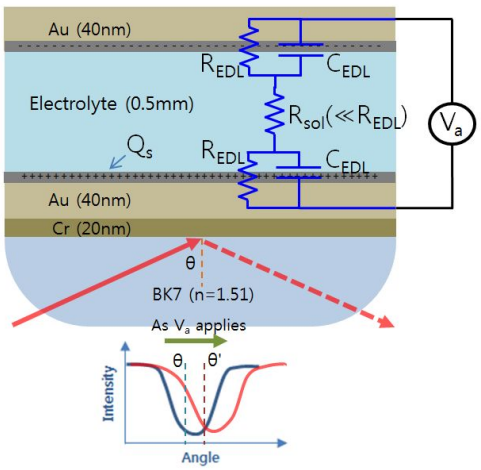

(a)

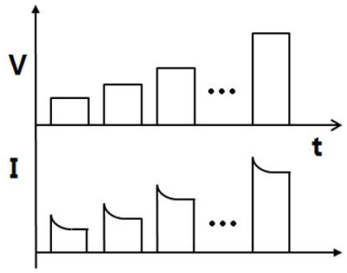

(b)

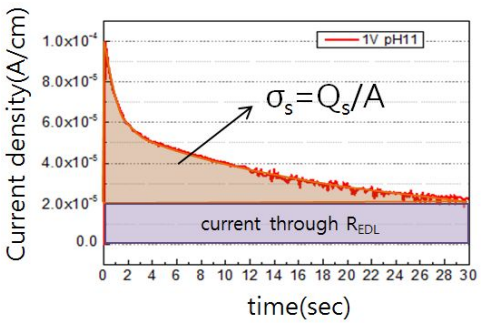

(c)

Fig. 3.9 SPR sensor experiment scheme (a) Experimental setup for our experiment. We make metal-solution-metal capacitor structure. We apply voltage between this capacitor, SPR angle changes from Θ to Θ'. (b) Pulsed voltage signal array and the transient current response. Due to the EDL resistance, current still flow after charging the EDL capacitor. (c) By integrating the transient component, we can obtain the accumulated charge.

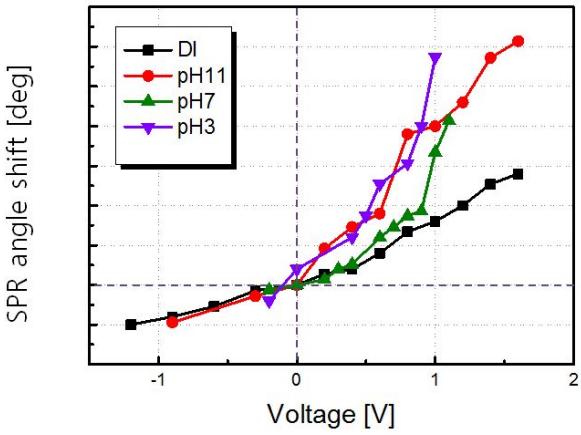

(a)

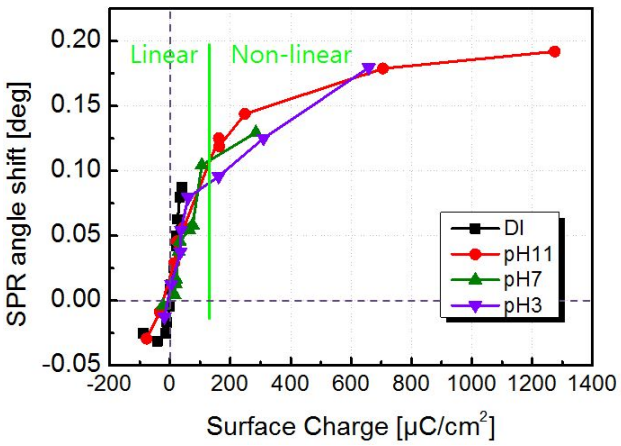

(b)

Fig. 3.10 SPR sensor experiment result (a) V vs. SPR angle shift (θ'-θ). (b) Surface charge density ve. SPR angel shift.

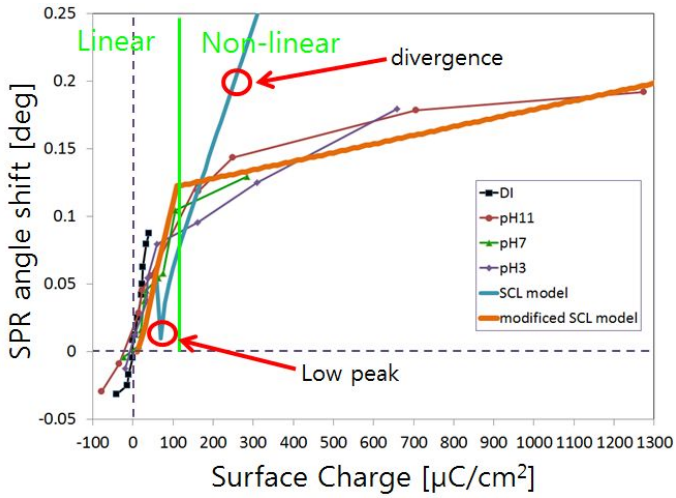

(a)

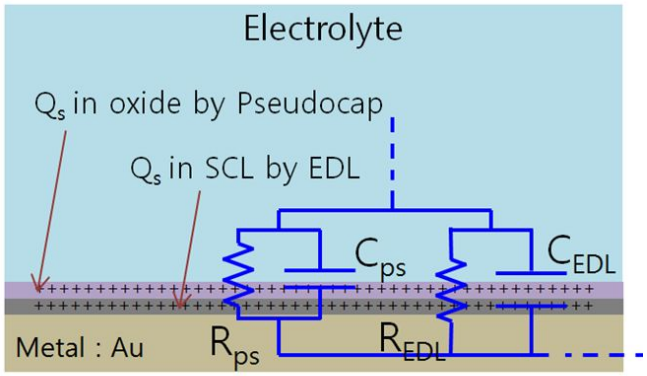

$$Au + 2H_2O \rightarrow AuOH \cdot H_2O + H^+ + e^- [1]$$

$$AuOH \rightarrow AuO + H^+ + e^- [1]$$

(b)

Fig. 3.11 SPR sensor experiment result (a) V vs. SPR angle shift (θ'-θ). (b) Surface charge density ve. SPR angel shift.

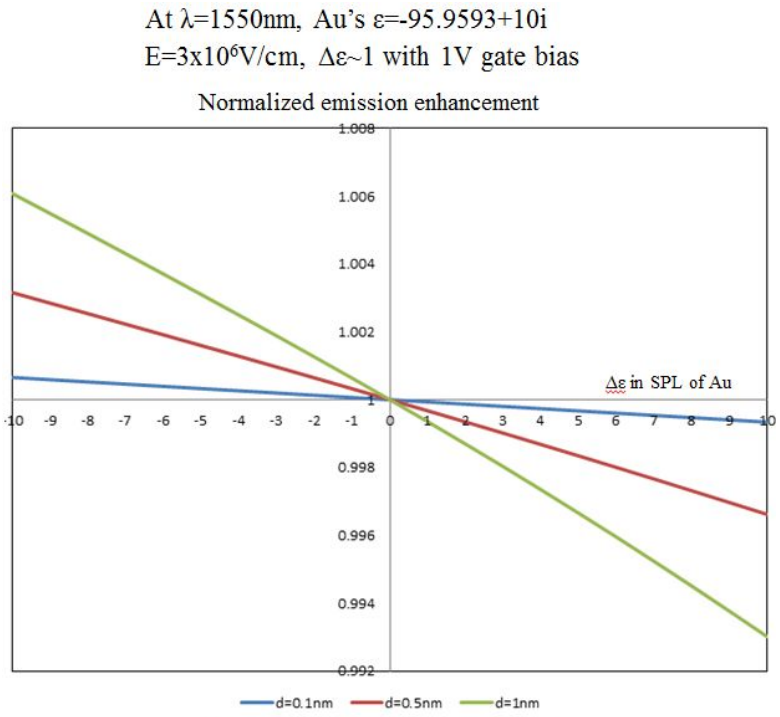

Fig. 3.12 Applying SCL model on fin LED. Optical modulation effect is not significant (~0.007 % Purcell factor change).

3.4 Physical analysis of 1D multilayer system

To investigate more physics for 1D multilayer system, we focus simpler model case, that is metal-dielectric system (Fig. 3.13(a)). As the emitter position from the metal d is closed, total LPDOS (total area) increases while the SP mode peak is sustained (Fig. 3.13(b)). The in-plain wave vector component of this peak coincide with SP mode in dispersion relation, as in section 3.1. But when the emitter is more closed to the metal less than 10 nm, the quenching effect occurs. This is increasement of LPDOS density in high in-plain k region (Fig. 3.13(c)). This corresponds to the loss by quenching. If we just plot total LPDOS not considering the quenching effect, LPDOS goes to infinite as d is closed to 0 (Fig. 3.13(d)).

If we decompose the LPDOS by integrating eq. (7) for different term, to SP enhanced part and quenching part (Fig. 3.14(a)). From this LPDOS component, we can obtain the enhanced quantum efficiency which consider the quenching effect. The quenching component does not enhance radiative spontaneous emission rate, it enlarge nonradiative decay (Fig. 3.14(b)). From this fact, we can obtain real quantum efficiency enhancement with quenching effect (Fig. 3.14(c)). Without quenching q goes to 1 as d goes to 0 because E goes to infinite and loss can be neglected. But actually the quenching effect ‘quench’ the emitter when the emitter is right beside the metal.

We apply this theory in our Fin Ge LED in Fig 3.15. The emitter

is located in Ge layer. As it is closed to the metal, the quenching effect will be larger. If it is at the interface between Ge and the oxide layer (Fig. 3.15(a)), we investigate LPDOS to see quenching effect. As oxide thickness is thinner than 5nm, the quenching effect is shown (Fig. 3.15(b)). This justifies our assumption that we can ignore the quenching effect in 5nm oxide thickness which is the oxide thickness of our device.

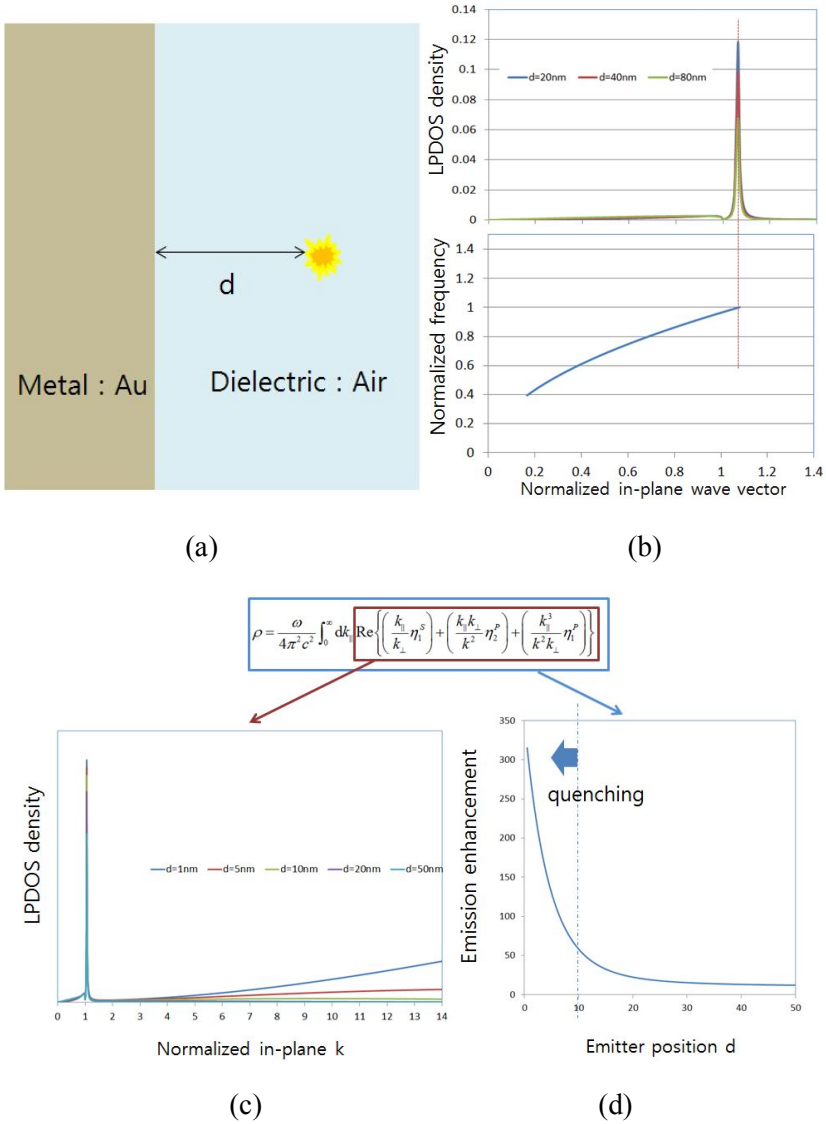

Fig. 3.13 Checking physical analysis for SP mode in 1D multilayer. (a) Model system which is simply metal-dielectric system. (b) Top : In-plane wave vector vs LPDOS density. Bottom : dispersion relation of this system. (c) In-pane wave vector vs. LPDOS density as emitter is closed to the metal surface. (d) Emitter position vs. LPDOS

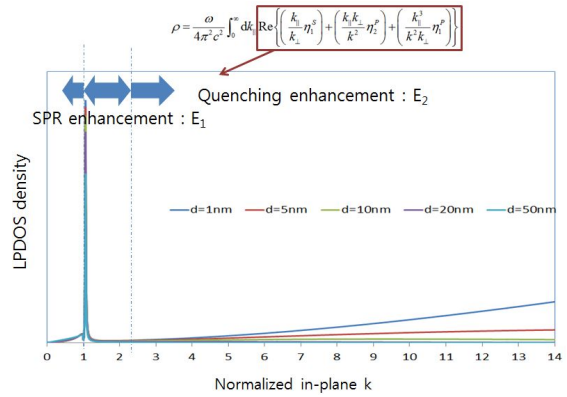

(a)

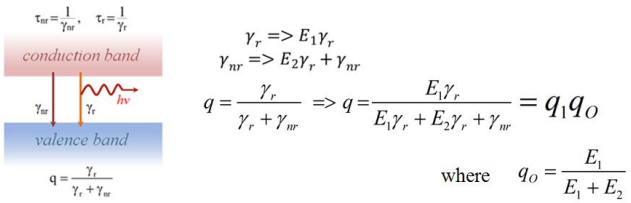

(b)

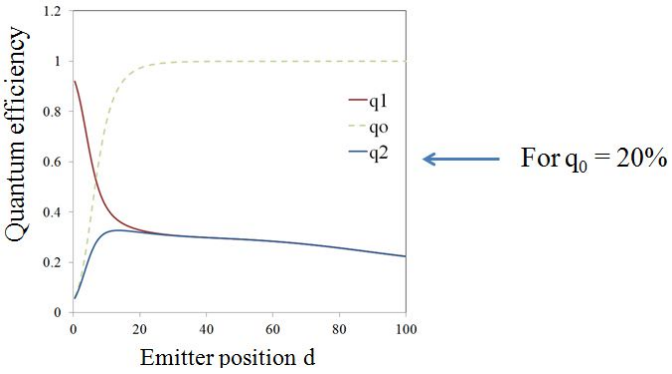

(c)

Fig. 3.14 (a) In-pane wave vector vs. LPDOS revisited. (b) Quantum efficiency considering the quenching effect. (c) Emitter position d vs. quantum efficiency for q_0=20%.

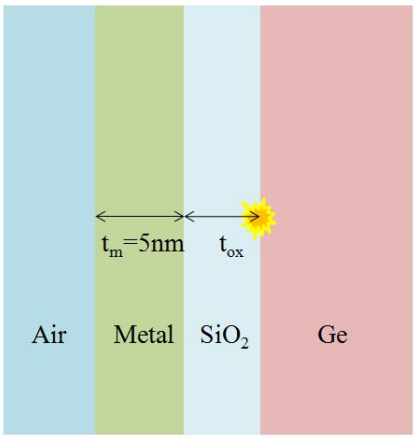

(a)

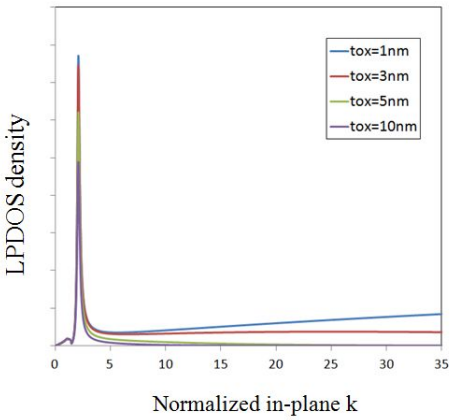

(b)

Fig. 3.15 (a) 1D multilayer system which is to see quenching aspect of our fin Ge LED. the emitter is at the interface between the oxdie and Ge layer (b) Quenching effect for this system. About t=5nm, quenching effect is shown. This justifies our assumption that we can ignore the quenching effect in 5nm oxide thickness which is the oxide thickness of our device.

3.5 Other considerations

In this section, we'll investigate other considerations like surface roughness effect and stress releasing and stress engineering.

To take into account the surface morphology of metal interface in 1D multilayer system, we need to know the root-mean squared (RMS) height of metal in metal-dielectric interface (Fig. 3.16). And from the surface roughness approximation theory[41], we can insert heterosystem layer at the interface and each metal and dielctric layer can be considered in this layer with weighted optical property from the theory. That means, rough surface in 1D multilayer system can be approximated as flat layer like other layers in 1D multilayer system.

Second, if we make pattern of fin array by etching, stress may be released in the normal direction of layered system. But if fin array is patterned like "bridge" structure (Fig. 3.17(a)), normal directional stress releasing can increase in-plane stress instead [45]. Further more gap-filling material like SiN_x can be stressor of fin structure (Fig. 3.17(b)) [46]. These two facts mean that stress and strain condition in fin structure can be engineered by patterning and gap-filling. This method can be applied in manufacturing of our device.

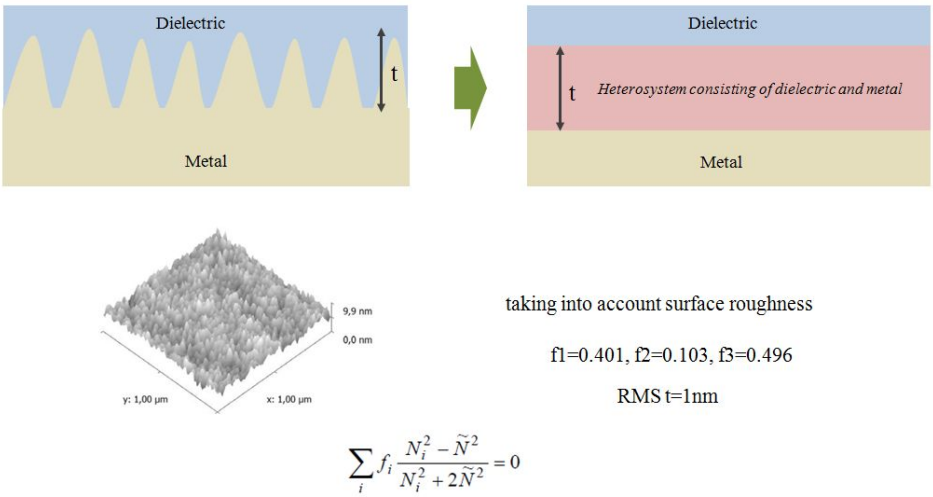

Fig. 3.16 Surface roughness approximation theory. The morphology of the surface can be taken into account in the 1D multilayer system. If we know the RMS (root-mean squared) value of surface height of which a heterogeneous layer system consisting of dielectric and metal can be constructed as approximated system.

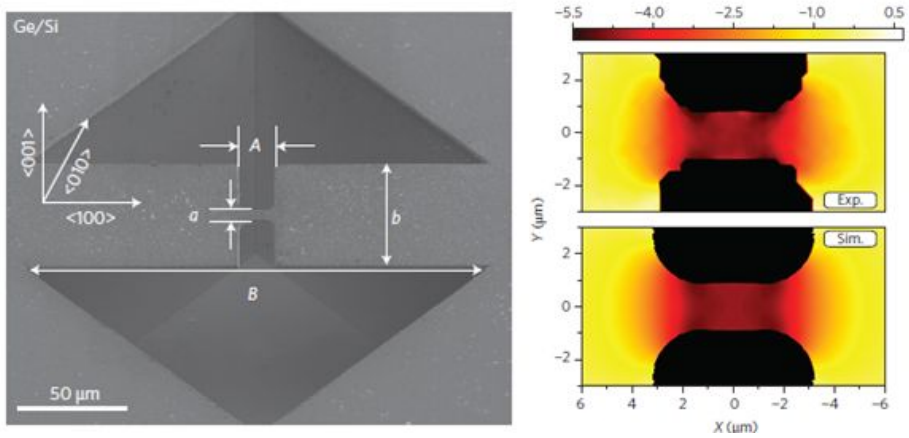

(a)

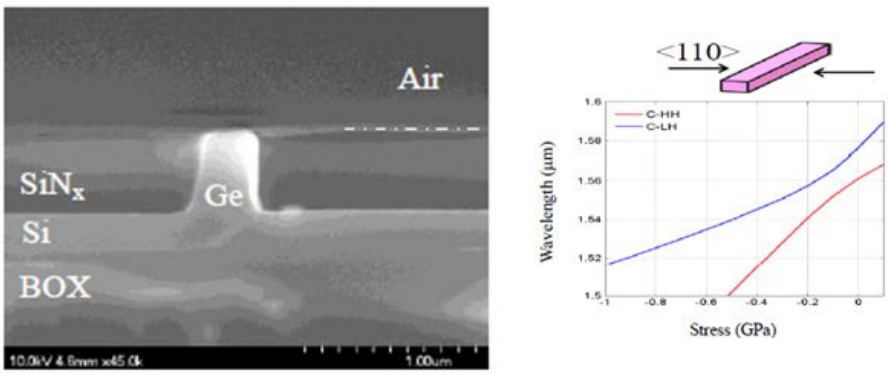

(b)

Fig. 3.17 Stress engineering (a) Bridge-like patterning can enhance uniaxial strain from biaxially stressed wafer. (b) Stress and strain on Ge can be engineered using stressors like SiN_x layer.

Chapter 4. Conclusion

4.1 Summary

Si photonics is the solution for bandwidth problem in future IC technology. All optical components except moderate on-chip light have been established monolithically until now. Ge has been a good candidate as material for on-chip light source in Si photonics since late 2000'.

We have proposed a fin Ge-Si LED with metal gates by which the spontaneous emission and quantum efficiency are enhanced due to coupling with surface plasmon resonant modes. In addition, the emitted light can be modulated directly by the gate voltage by controlling the injection of the carriers in the diode. Through the analysis based on numerical simulations, it has been shown that the enhancement of the light and gate modulation is dependent on the device dimensions such as the fin semiconductor thickness, gate oxide and the metal thickness. Our device can be an efficient on-chip monolithic Ge light source for Si photonics systems.

Two aspects of gate modulation, that is electrical and optical, are investigated. We show electrical modulation is possible with 5 GHz speed, which is the same speed of the direct modulation. By

conducting experiment with SPR sensor, we show the relation between the surface charge in the metal surface and SPR angle, which is related to optical property of the metal. Also we construct a model that explains our experimental result. From our model, optical modulation effect in the fin Ge LED is not significant and we don't need to consider it more.

We carefully investigate 1D multilayer system including metal layer to understand the physics of our device well.

Furthermore, the analysis methods proposed in this paper can be extended to designing not only the fin Ge-Si LED but also any surface plasmon-enhanced LEDs and nano-cavity lasers [34].

4.2 Future works

As future works, calculations based on the three-dimensional finite element method are needed to obtain the exact dyadic Green's function and the LPDOS of the emitter for estimation of the spontaneous emission enhancement in arbitrary device structures such as a pillar structure (Fig. (a)) providing more localized light emission.

Also, before manufacturing the real device, we can check our theory by PL (photoluminescence) experiment with simpler device structure (Fig. (b)). We just need a Ge fin array with various fin thickness and deposit metal on this array with various thickness. Then PL experiment will verify our result that the spontaneous emission rate is a function of device dimension.

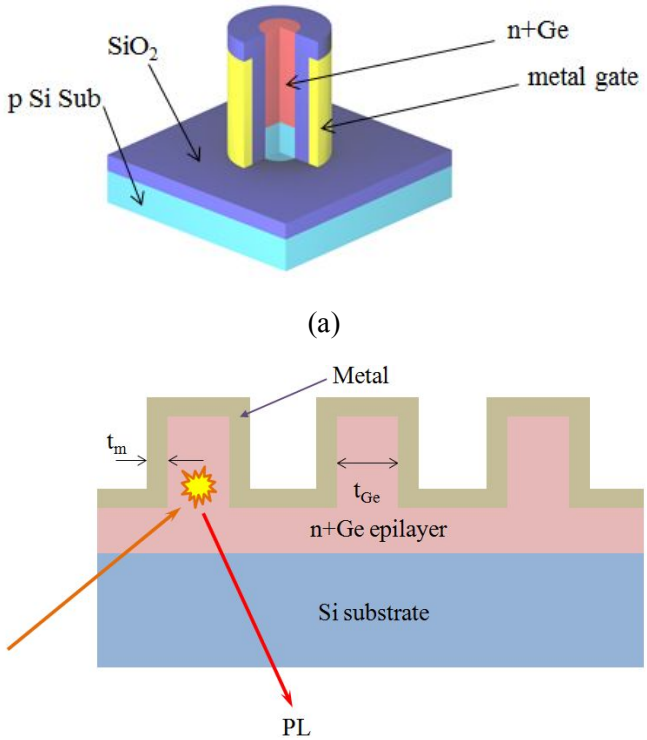

Fig. 4.1 Future workds (a) Pillar structure version of our fin Ge-Si LED. We can't use multilayer approximation in this case. If we can obtain the system's dyadic Green's function (eq. (4)) even for an arbitrary structure like this, we can obtain the same calculation with the result from 1D multilayer conjecture. 3D FEM or FDTD can be applied to accquire Green's function. (b) PL experiment scheme. We need just Ge fin array on Si substrate and metal deposition. This can verify our theory.

References

1. L. Tsybeskov, D. J. Lockwood, and M. Ichikawa, "Silicon photonics: CMOS going optical," Proc. IEEE 97, 1161-1165 (2007).
2. R. Soref, "The past, present, and future of silicon photonics," IEEE J. Sel. Top. Quantum Electron. 12, 1678-1687 (2006).
3. Z. Fang and C. Z. Zhao, "Recent progress in silicon photonics: a review," ISRN Optics 2012 428690 (2012).
4. G. T. Reed, Silicon photonics: The state of the art (John Wiley and Sons Inc, 2008).
5. G. T. Reed, G. Mashanovich, F. Y. Gardes, and D. J. Thomson, "Silicon optical modulators," Nat. Photon. 4, 518-526 (2010).
6. L. Liao, D. Samara-Rubio, M. Morse, A. Liu, and D. Hodge, "High speed silicon Mach-Zehnder modulator," Opt. Express 13, 3129-3135 (2005).
7. J. Michel, J. Liu, and L. C. Kimerling, "High-performance Ge-on-Si photodetectors," Nat. Photon. 4, 527-534 (2010).
8. J. Leuthold, C. Koos, and W. Freude, "Nonlinear silicon

photonics," Nat. Photon. 4, 535-544 (2010).

9. A. W. Fang, H. Park, O. Cohen, R. Jones, M. J. Paniccia, and J. E. Bowers, "Electrically pumped hybrid AlGaInAs-silicon evanescent laser," Opt. Express 14, 9203-9210 (2006).

10. G. Roelkens, L. Liu, D. Liang, R. Jones, A. Fang, B. Koch, and J. Bowers, "III-V/silicon photonics for on-chip and intra-chip optical interconnects," Laser Photon. Rev. 4, 751-779 (2010).

11. J. Liu, X. Sun, D. Pan, X. Wang, L. C. Kimerling, T. L. Koch, and J. Michel, "Tensile-strained, n-type Ge as a gain medium for monolithic laser integration on Si," Opt. Express 15, 11272-11277 (2007).

12. C. W. Liu, T. Cheng, Y. Chen, S. Jan, C. Chen, S. Chan, Y. Nien, Y. Yamamoto, and B. Tillack, "Direct and indirect radiative recombination from Ge," Thin Solid Films 520, 3249-3254 (2012).

13. R. E. Camacho-Aguilera, Y. Cai, N. Patel, J. T. Bessette, M. Romagnoli, L. C. Kimerling, and J. Michel, "An electrically pumped germanium laser," Opt. Express 20, 11316-11320 (2012).

14. X. Sun, J. Liu, L. C. Kimerling, and J. Michel, "Room-temperature direct bandgap electroluminescence from Ge-on-Si light-emitting diodes," Opt. Lett. 34, 1198-1200 (2009).

15. S. Cheng, J. Lu, G. Shambat, H. Yu, K. Saraswat, J. Vuckovic, and Y. Nishi, "Room temperature 1.6 μm electroluminescence from Ge light emitting diode on Si substrate," Opt. Express 17, 10019-10024 (2009).

16. F. Zhang and V. H. Crespi, "Prediction that uniaxial tension along <111> produces a direct band gap in germanium," Phys. Rev. Lett. 102, 156401 (2009).

17. J. Liu, X. Sun, R. Camacho-Aguilera, Y. Cai1, L. C. Kimerling, and J. Michel, "Monolithic Ge-on-Si lasers for integrated photonics," presented at the IEEE 7th International Conference on Group IV Photonics, Beijing, China, 1-3 Sept. 2010.

18. S. M. Sze and K. Kwok, Physics of semiconductor devices (John Wiley and Sons Inc, 2007).

19. S. Pillai, K. R. Catchpole, T. Trupke, G. Zhang, J. Zhao, and M. A. Green, "Enhanced emission from Si-based light-emitting diodes using surface plasmons," Appl. Phys. Lett. 88, 161102 (2006).

20. D. M. Schaadt, B. Feng, and E. T. Yu, "Enhanced semiconductor optical absorption via surface plasmon excitation in metal nanoparticles," Appl. Phys. Lett. 86, 063106 (2005).

21. K. Okamoto, I. Niki, A. Shvartser, Y. Narukawa, T. Mukai, and

A. Scherer, "Surface-plasmon-enhanced light emitters based on InGaN quantum wells," Nat. Mat. 3, 601-605 (2004).

22. E. M. Purcell, "Spontaneous emission probabilities at radio frequencies," Phys. Rev. 69, 681 (1946).
23. K. Nozaki, S. Kita, and T. Baba, "Room temperature continuous wave operation and controlled spontaneous emission in ultrasmall photonic crystal nanolaser," Opt. Express 15, 7506-7514 (2007).
24. P. Anger, P. Bharadwaj, and L. Novotny, "Enhancement and quenching of single-molecule fluorescence," Phys. Rev. Lett. 96, 113002 (2006).
25. J. R. Lakowicz, "Radiative decay engineering: biophysical and biomedical applications," Anal. Biochem. 298, 1-24 (2001).
26. H. T. Miyazaki, "Squeezing visible light waves into a 3-nm-thick and 55-nm-long plasmon cavity," Phys. Rev. Lett. 96, 097401 (2006).
27. L. Novotny and B. Hecht, Principles of nano-optics (Cambridge University Press, 2006).
28. K. Joulain, R. Charminati, J. Mulet, and J. Greffetm "Definition and measurement of the local density of electromagnetic states close to an interface," Phys. Rev. B 68, 245405 (2003).

29. I. Jeoug, C. Kim, and Y. J. Park, "Numerical analysis of surface-plasmon-enhanced light emission in fin silicon light-emitting diode," presented at the IEEE 7th International Conference on Group IV Photonics, Beijing, China, 1-3 Sept. 2010.

30. M. Tomas, "Green function for multilayers: Light scattering in planar cavities," Phys. Rev. A 51, 2545-2559 (1995).

31. J. E. Sipe, "New green-function formalism for surface optics," J. Opt. Soc. Am. B 4, 481-489 (1987).

32. J. Kwon, I. Jeong, S. Choi, and Y. J. Park, "An embedded modulation of GeSi fin LED - A simulation study," presented at the 10th International Workshop on Compact Modeling, Yokohama, Japan, 22 Jan. 2013.

33. L. M. Brekhovskikh, Waves in layered media, 2nd ed. (Academic Press, 1980).

34. S. Chang, C. Ni, and S. L. Chuang, "Theory for bowtie plasmonic nanolasers," Opt. Express 16, 10580-10595 (2008).

35. W. L. Barnes, A. Dereux, and T. W. Ebbesen, “Surface plasmon subwavelength optics,” Nat. **424**, 824-830 (2005).

36. S. A. Maier, “Plasmonics : Fundamentals and Applications,” (Springer Science+Business Media LLC, Spring Street NY, USA,

2007).

37. J. Homola, S. S. Yee, and G. Gauglitz, “Surface plasmon resonance sensors: review,” Sensors and Actuature B **54** 3-15 (1999).

38. Y. Ryu, T. Son, and D. Kim, “Near-field evaluation of surface plasmon resonance biosensor sensitivity,” Korean Journal of Opt. and Photon. **24**, 86-91 (2013)

39. J. E. Garland, K. A. Assionbon, C. M. Pettit, and D. Roy, “Surface plasmon resonance transients at an electrochemical interface: time resolved measurements using a bicell photodiode,” Anal. Chim. Acta **475** 47-58 (2003).

40. V. Lioubimov, A. Kolomenskii, A. Mershin, D. V. Nanopoulos, and H. A. Schuessler, “Effect of varying electric potential on surface-plasmon resonance sensing,” Appl. Opt. **43** 3426-3432 (2004).

41. A. M. Lopatynskyi, O. G. Lopatynska, M. D. Guiver, L.V. Poperenko, V. I. Chegel, “Factor of interfacial potential for the surface plasmon-polariton resonance sensor response,” Semicon. Phys. Quant. Electron. & Opt. **11** 329-336 (2008).

42. J. D. E. McIntyre, “Electrochemical modulation spectroscopy,” Surf. Sci. **37** 658-682 (2004).

43. B. E. Conway, V. Birss, and J. Wojtowicz, “The role and utilization of pseudocapacitance for energy storage by supercapacitors,” Journal of Power. Sources **66** 1-14 (1997).

44. MiCoBioMed, AMiCo Company http://www.micobiomed.com/html/SPR_principle.php

45. M. J. Suess, *et al,* "Analysis of enhanced light emission from highly strained germanium microbridges" *Nature Photon.* (2013)

46. L. Nguyen, et al, "Strain tuning of pure Germanium for Franz-Keldysh electro-absorption modulation", *IEEE Group IV Photon.* (2013)

요약(국문초록)

표면 플라즈몬에 의해 증폭된 Fin Ge-Si 발광 다이오드의 설계와 분석

서울대학교

융합과학기술대학원

융합과학과 나노융합전공

정인태

실리콘 포토닉스(Si photonics)는 포토닉 소자들을 CMOS칩 안에 집적시키는 것에 대한 분야로, 모듈레이터, 도파로, 디텍터 등을 포함한 거의 모든 포토닉 소자들이 상업적으로 잘 구현되어 있다. 그러나 효율적인 4족원소 공정에 잘 맞는 칩내의 광원은 그렇지 못해 학계에서 아직 활발히 연구중인 상태이다. 다행히 강하게 도핑된 스

트레인을 받는 저마늄(Ge)이 의사 직접 천이 밴드 갭 때문에 빛을 비교적 효율적으로 낼 수 있고, 이러한 성질이 Ge를 실리콘 포토닉스 시스템의 좋은 광원후보로 만들게 한다. 본 논문에서 저자는 핀(fin)모양에 양쪽에 금속 게이트가 있어서 표면 플라즈몬 공명(Surface plasmon resonance) 모드와 결합해 빛을 증폭시키고, 나오는 빛을 조절할 수 있는 Ge-Si 이종접합 발광다이오드(LED)를 제안하였다. 이 증폭효과는 소위 퍼셀효과로 불리고, 이 효과 때문에 발광원의 자발 발광(Spontaneous emission)률이 금속 동공(metal cavity)와 같은 자체의 환경에 영향을 받아 바뀔 수 있다. 저자가 제안한 소자에서 이 효과는 금속 게이트 표면의 표편 플라즈몬에 의해 야기된다. 우리는 우리의 핀 소자에서의 이러한 증폭효과를 계산하였고, 소자의 특정한 치수에서 자발 발광이 최대화가 될 수 있음을 보였다. 우리는 표면 플라즈몬 효과의 원리에 대한 더 깊은 이해를 위해 1차원 다중층 시스템의 물리에 대해 면밀히 분석하였다. 또한 전기적, 광학적 측면에서의 게이트 모듈레이션 효과를 점검하였다. 소자 시뮬레이션을 통해 우리는 5GHz의 속도의 전기적인 모듈레이션이 가능함을 보였다. 표면 플라즈몬 공명 센서를 통한 실험을 수행하여 광학적인 모듈레이션에 대해서도 확인해 보았다. 센서의 금속전극에 전압을 가한 후 표면 플라즈몬 공명 각도의 변화를 관측하였고, 실

험결과를 설명하는 모델을 세우고 본 소자에 적용하였다. 그 결과 광학적인 측면에서의 증폭의 조절을 잘 되지 않음을 확인했다. 이 연구는 Si photonics 시스템의 칩 내부의, 표면 플라즈몬에 의해 증폭된 LED 또는 나노동공(nanocavity) 레이저와 같은 광원의 설계와 최적화를 하는데 있어서 큰 도움이 될 것이다.

주요어 : 표면 플라즈몬 공명, 퍼셀 효과, 게이트 모듈레이션, 실리콘 포토닉스, 저마늄 광원

학 번 : 2009-30731